## ORIGINAL ARTICLE

# Fabrication of Nb/V co-doped TiO$_2$ thin films and study of structural, optical and photocatalytic properties

*Behzad Koozegar Kaleji[1]\*; Navid Alami Fariman[1]; Navid Hosseinabadi[2]*

*[1]Department of Materials Engineering, Faculty of Engineering, Malayer University, Malayer, Iran*
*[2]Department of Materials Engineering and Metallurgy, Faculty of Engineering, IAU-Shiraz Branch, Shiraz, Iran*

**Abstract**
In this study, different samples of Niobium and Vanadium co-doped titania thin films (5-10-15 mol% Nb and 5-10-15 mol% V) were prepared via sol–gel dip coating method, using niobium chloride as niobium precursor, ammonium metavanadate as vanadium precursor, and titanium (IV) butoxide (TBT) as titanium precursor. The effects of doping amount on the structural, optical, and photo-catalytic properties of formed thin films have been studied by X-ray diffraction (XRD), scanning electron microscopy (SEM), UV-Vis absorption and transmission electron microscopy (TEM). XRD patterns showed a decrease in peak intensities of the anatase crystalline phase by increasing the Nb/V dopant and doping inhibition effect on the grain growth, and revealed that all samples contained only anatase phase (T= 475 °C). The photo-catalytic activity of the thin film was measured on degradation rate of methylene blue (MB) solution under UV irradiation. Highest photo-catalytic activity of doped TiO$_2$ thin films were measured in the TiO$_2$–5 mol% Nb-15 mol% V sample (TNV4). Small granular crystallites of 10-15 nm 2D diameter were observed in electron microscope micrographs.

**Keywords:** *Nb/V dopant; Optical properties; Sol-Gel; Thin film; TiO$_2$.*

## INTRODUCTION

The titanium dioxide has been widely used in the field of pollutant degradation and environment protection since photo-catalytic function of titania was discovered in 1972 [1, 2]. The titanium dioxide has the advantage of not only high photo-catalytic activity, but also good acid resistance, low cost, and no toxicity, which makes the titanium dioxide become one of the best photo-catalytic agents [3, 4]. TiO$_2$ can catalytically decompose a large number of organic and inorganic pollutants under illumination of UV light [5-7]. However, depending on the structural form, the photo-catalytic activity of TiO$_2$ has been found to vary.

Lin *et al.* [8] and Maruska and Ghosh [9] have related the higher photoactivity of anatase TiO$_2$ (E$_g$ = 3.2 eV) to its higher Fermi level compared to that of rutile TiO$_2$ (E$_g$ = 3.0 eV). However,

high photocatalytic activity has been reported with multi-phased mesoporous TiO$_2$, consisting of anatase and rutile [10, 11]. Thus, more investigations seem necessary to understand the effect of metal ion doping on the structural and optical properties of TiO$_2$.

Dopants, such as transitional metals can be added to TiO$_2$ to improve its catalytic activity and also reduce the recombination of photo-generated electrons and photo-generated holes. Noble metals doped or deposited on TiO$_2$ also show effect on the photocatalytic activity by extending excitation wavelength from the UV to the visible light range [12–21].

Alumina, silica, and zirconia have been used to stabilize anatase [22–24]. It has been suggested that Al, Si, and Zr stabilize anatase by occupying interstices, thereby distorting the anatase lattice

* Corresponding Author Email: *bkaleji@yahoo.com*

and restricting the lattice contraction involved in the transformation to rutile.

Karakitsou and Verykios [25] showed that doping with cations having a valence higher than +4 can increase the photoactivity, whereas Mu *et al.* [26] reported that doping with trivalent or pentavalent metal ions was detrimental to the photoactivity even in the UV region. Furthermore, according to a systematic study on the photoactivity and transient absorption spectra of quantum-sized $TiO_2$ doped with 21 different metals the energy level and d-electron configuration of the dopants were found to govern the photo electrochemical process in $TiO_2$ [27]. Even though the effects of metal doping on the activity of $TiO_2$ have been a frequent topic of investigation, it remains difficult to make unifiable conclusion on the effects of doping on photoactivities of $TiO_2$.

The choice of the doping type may play a crucial role in the crystalline structure and the stable phase of $TiO_2$ thin films. The metal ions which are found to inhibit the anatase to rutile phase transformation are Si [28] and Cr [29], while the metal ions which are reported to promote the phase transformation are Ni, Co, Mn, Fe, Cu [30], Ag [31], S [18] and N [21].

In the present work, Nb/V co-doped $TiO_2$ thin films were applied by sol-gel dip-coating process. Effects of co-doping on the structure, optical and photo-catalytic properties of titania thin films has been studied. The photocatalytic performance of the Nb/V co-doped $TiO_2$ thin film was evaluated by photo degradation MB solution (Methylene Blue) under UV light irradiation. In addition, the influence of calcination temperature (475 °C, 575 °C, 675 °C) on the structural and optical properties of the prepared $TiO_2$ thin films was investigated.

## EXPERIMENTAL
### Preparation of the thin films

The preparation of precursor solution for Nb/V co-doped $TiO_2$ thin film is described as follows: Titania, Niobium oxide and Vanadium oxide sols were prepared, separately. For the preparation of $TiO_2$ sol, titanium (IV) butoxide (TBT=$Ti(OC_4H_9)_4$, Aldrich) was selected as titanium source. First, 0.35 mol ethanol (EtOH, Merck) and 0.04 mol ethyl acetoacetate (EAcAc is as a sol stabilizer during preparation of sol, Merck) were mixed, and then 0.01 mol TBT was added by the rate of 1 ml/min to the mixture at the ambient temperature (25 °C). The solution was continuously stirred for

45 min, followed by dropping of $HNO_3$ as catalyst to the solution until pH of 3. De-ionized water was added to the solution slowly to initiate hydrolysis process. Solution was aged for 24 h in order to complete all reactions. The chemical composition of the resultant alkoxide solution was TBT: $H_2O$: $HNO_3$: EAcAc: EtOH=1: 10: 1: 4: 35 in molar ratio.

In order to prepare niobium and vanadium oxide sols, niobium chloride ($NbCl_5$, Merck) and ammonium metavanadate ($NH_4VO_3$, Merck), were dissolved in EtOH with molar ratio of $NH_4VO_3$: EtOH = 1:35 and $NbCl_5$: EtOH = 1:35 at ambient temperature with continuous stirring. Solutions were aged for 24 h in order to complete all reactions. Then, mixtures of titania sol, niobium precursor sol and vanadium precursor sol were made with different mole percent of Nb and V at the ambient temperature.

Before coating, the glass substrates (15 × 50 × 1 mm) were cleaned with ethanol. Thin films were prepared by a dip coating method. The withdrawn speed was 1 cm/min. The gel films were air dried for 1 h, and then heat-treated at 475 °C for 1 h in air (heating rate; 5 °C/min).

The final product's molar content of Nb and V, was set to change from 5 mol%, 10 mol%, 15 mol% for Nb and V was set to change between 5 mol%, 10 mol%, 15 mol% (Samples code: TNV1: 5%Nb-5%V, TNV2: 10%Nb-10%V, TNV3: 15%Nb-15%V, TNV4: 5%Nb-15%V, TNV5: 15%Nb-5%V).

### Characterization methods

XRD pattern and phase identification of thin films were recorded using X-ray diffraction analysis (Philips, MPD-XPERT, $\lambda$ : $Cu_{k\alpha}$ = 0.154 nm). The samples were scanned in the 2θ range of 20-80°. Morphology of the thin films was observed using scanning electron microscopy (SEM, XL30 Series) with an accelerating voltage of 10–15 kV. Energy-dispersive X-ray analysis (EDX, voltage 20 KV, Take off Angle 35.0) was also used for the chemical analysis of the thin films. In order to make TEM foils, the films were removed from the substrates by water flotation. Droplets of the sol-gel material were also deposited on plain (un-coated) copper grids to form free-standing films for in-situ hot-stage experiments in the TEM. Conventional TEM imaging and electron diffraction analysis was carried out using an EM-2100F-JEOL-Tokyo-Japan with acceleration voltage of 200 kV.

The specific surface area of the samples was evaluated using the BET method. The BET surface

area was determined by nitrogen adsorption–desorption isotherm measurement at 77 °K. The sample was degassed at 150 °C prior to actual measurement.

*Photo-catalytic activity measurement*

The photo-catalytic activity was evaluated by monitoring the degradation of MB solution (10 ppm) under UV illumination. The samples were placed in 20 ml aqueous MB solution and kept in dark for 1 h. Then, have irradiated from top by using a UV lamp (Philips 8W, 365 nm). The intensity of the MB characteristic band at 664 nm ($I_{664}$) in the obtained UV–vis spectrum (Varian cary 50 spectrophotometer) was used to determine the concentration of MB in the solution ($C_t$).

The degradation percentage of MB, which represents the photo-catalytic efficiency of the films, can be determined by equation 1.

$$\eta(\%) = \left[ \frac{A_0 - A_t}{A_0} \right] \times 100 \qquad (1)$$

Where is degradation percentage of MB, $A_t$ is Absorption after radiation and $A_0$ is Absorption before radiation [32].

The amount of rutile in the samples was calculated using equation: [33]

$$X_R = (1 + \frac{0.8 I_A}{I_R})^{-1} \qquad (2)$$

where $X_R$ is the mass fraction of rutile in the samples, and $I_A$ and $I_R$ are the X-ray integrated intensities of (1 0 1) reflection of the anatase and (1 1 0) reflection of rutile, respectively.

**RESULTS AND DISCUSSION**

Fig. 1 shows the XRD patterns of the thin films with Nb and V doped samples calcined at 475 ºC for 1h. The peaks at 25.3°, 37.7°, 48.1°, 53.8° and 62.4° in all doped samples belongs to (101), (004), (200), (105) and (213) planes of anatase phase of $TiO_2$. In addition, all samples (Table 1, %A=100) were identified as polymorphs of anatase (JCPDS: No. 21-1272), without any significant impurity phases. No characteristic peaks of $Nb_2O_5$ were observed in doped $TiO_2$ thin films, which suggest the incorporation of $Nb^{5+}$ into the $TiO_2$ lattice [34]. Also, no significant characteristic peaks of vanadium based phases were found in corresponding XRD patterns. Results from numerous reports have shown that the incorporation of transition metal ions into other compounds as dopants could distort the original crystal lattice of the base

materials [35]. The peak position of the co-doped TNV samples gradually shifted towards a higher diffraction angle. It suggests that the V ions might be successfully incorporated into the crystal lattice of anatase $TiO_2$ as vanadyl groups ($V^{4+}$) or polymeric vanadates ($V^{5+}$) and substituted for $Ti^{4+}$ because the ionic radii of $V^{4+}$ (0.72 Å) and $V^{5+}$ (0.68 Å) were both slightly smaller than that of $Ti^{4+}$ (0.75 Å) [36].

Also, the XRD measurements showed that both $TiO_2$ and co-doped doped $TiO_2$ thin film contain only anatase phase. The structure of co-doped $TiO_2$ film has lower crystallinity relative to pure sample [34].

The intensity of the X-ray diffraction lines decreases slightly with the increase of dopant content. In Nb/V-doped $TiO_2$ films, no $TiO_2$ polymorphs or V-based or Nb-based compounds were detected within instrumental limits. However, the effect of the dopant presence on their crystallization tendency is observed.

In high amounts of Nb and low amounts of V in the samples (TNV3, TNV5), the crystallization is close to the amorphous phase. However, an increase in the crystallization behavior is observed for the TNV4 samples. Hence these results imply that co-doping with Nb and V in $TiO_2$ not only suppresses the formation of any impurity phase but also prevents phase transition from anatase to rutile.

Also, a considerably lower intensity of anatase peak was detected in the doped sample (TNV3, TNV5) in comparison to the undoped sample. Consequently, it was implied that increasing of dopant concentration could decrease the intensity of anatase phase. It is found that the Nb/V dopants can inhibit the anatase grain growth and promote an amorphous phase formation (TNV3, TNV5).

The average crystallite size (Table 1) of thin films (d) was determined from the XRD patterns, according to the Scherrer equation (3) [33]

$$d(nm) = \frac{k\lambda}{\beta \cos\theta} \qquad (3)$$

where k is a constant (shape factor, about 0.9), λ the X-ray wavelength (0.154 nm), β the full width at half maximum (FWHM) of the diffraction peak and θ is the diffraction angle. The values of β and θ of anatase and rutile phases were taken from anatase (1 0 1) and rutile (1 1 0) planes diffraction lines, respectively.

The decrease in crystallite size can be attributed to the presence of Nb and V in co-doped $TiO_2$ thin

films which inhibits the growth of crystal grains. According to Table 1, surface area of the co-doped $TiO_2$ thin film relative to pure samples has increased by increasing both Nb and V content (except TNV5). However, the main difference is in the rate of surface area increase. A maximum surface area of 171.3 $m^2$/g was measured for TVN2 sample.

According to Fig. 2, the order of photo-catalytic activity of pure and co-doped thin films at 1h under UV irradiation is as follows: TNV4 >TNV1> TNV2 > T > TNV3 > TNV5, which suggests that the doping enhances the photo-catalytic activity of thin films. This enhanced photocatalytic activity is because of suppressed recombination of photogenerated electrons and holes.

It was apparent that dopant was highly effective on degradation of MB solution since the pure $TiO_2$ thin film (T) had photocatalytic activity. Addition of doping would improve UV light attraction, and hence improve the photocatalytic activity under irradiation. Degradation of MB generally improved with increasing crystallization (maximum crystallinity=TNV4) and surface area.

The reported optical band gap ($E_g$) in Fig. 3 has been calculated using the UV–vis spectra by:

$$\alpha h\upsilon = A(h\upsilon - E_g)^n \tag{4}$$

Where *hv* is the photon energy, A and n are constants. For allowed direct transition n = 1/2, direct forbidden transition n = 3/2 and indirect allowed transition n = 2 [37]. The optical band
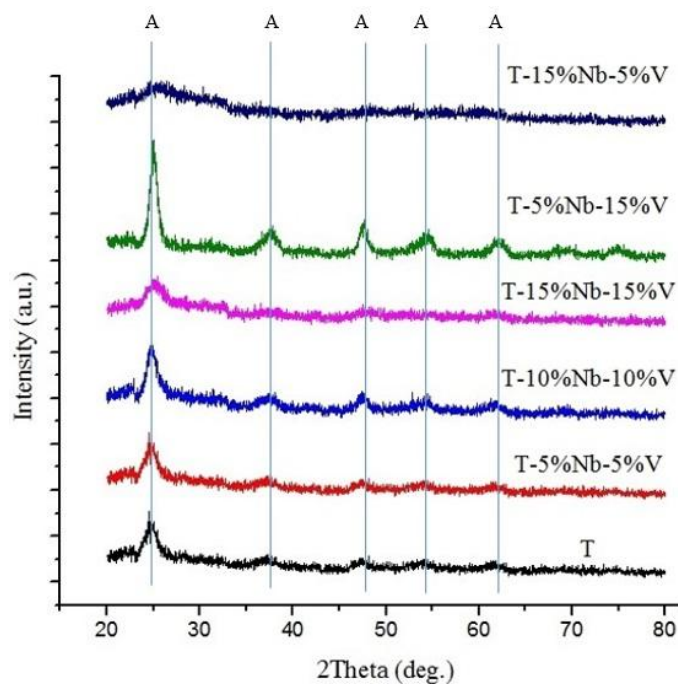


Fig. 1: XRD patterns of the pure and Nb/V co-doped $TiO_2$ thin film calcined at 475 ºC.

Table 1: characteristic of pure (T) and doped TiO2 (TNV) thin film at 475 ºC and 1h. (d: crystallite size (nm), %A: Aamount of anatase phase, %R: amount of rutile phase, $d_A$: Crystallite size of anatase, $d_R$: Crystallite size of rutile, BET : Specific surface area)

| Sample code | Nb (mole %) | V (mole %) | %A | %R | $d_A$ (nm) | $d_R$ (nm) | BET ($m^2$/g) |
|---|---|---|---|---|---|---|---|
| T | -- | -- | 100 | -- | 18.2 | -- | 86.1 |
| TNV1 | 5 | 5 | 100 | -- | 9.3 | -- | 167.7 |
| TNV2 | 10 | 10 | 100 | -- | 8.2 | -- | 171.3 |
| TNV3 | 15 | 15 | 100 | -- | 6.4 | -- | 106.4 |
| TNV4 | 5 | 15 | 100 | -- | 11.1 | -- | 158.2 |
| TNV5 | 15 | 5 | 100 | -- | 4.6 | -- | 71.8 |

*B. Koozegar Kaleji et al.*

gap Energy ($E_g$) is estimated by extrapolating the straight line portion of $(\alpha h\nu)^{1/n}$ with the abscissa axis ($h\nu$) in the vicinity of the fundamental optical transition for Nb/V co-doped thin film. The band gap of the pure $TiO_2$ thin film was 3.2 eV, which increased up to 3.42 eV with increasing dopant content. The widening of the band gap can be explained by the Burstein-Moss (BM) effect [38], in which the lowest states in the conduction band were blocked, and transitions can take place only to energies higher than Fermi energy. Thus, the band gap widens with increasing dopant content. The observed values were slightly higher than the band gap of both bulk and thin film $TiO_2$ in the anatase phase. The reported values were 3.18 eV [39] for bulk material and in the range 3.2-3.23 eV for thin films [40]. The higher band gap observed in our case can be associated with the nanocrystalline nature of the thin films.

The effects of calcination temperatures on the crystal structure and composition were investigated by XRD. Fig. 4 illustrates the XRD patterns of the TNV4 thin films calcined at various calcination temperatures for 1 h in air. As the temperature increased from 475 °C to 575 °C, the intensities of the anatase peaks were increased, implying an

improvement in crystallinity. By increasing the temperature to 675 °C, the intensities of the anatase peaks decreased and the rutile peaks was appeared. It can be seen that the mass fraction of rutile phase increases with increasing calcined temperature (Table 2). At 575 °C, the mass fraction of rutile is 26.6%, while at 675 °C, the content of rutile reaches up to 58.5%. Therefore, it is reasonable to deduce that a small amount of anatase phase is transformed into rutile phase during heat treatment. Usually, the increased calcination temperature can induce phase transformation from anatase to rutile and accelerate the growth of crystallites [41]. This effect can be found in Table 2 that the crystalline size of anatase and rutile increases with calcination temperatures.

Also, the crystallite size has increased but the surface area decreased with an increase of the calcination temperatures for TNV4 sample (Table 2).

Minimum surface area was measured about 56.8 $m^2$/g (T= 675 °C). It is common that the surface area decreases with the elevating calcination temperature due to the degree of crystallinity. In samples calcined at 675 °C, higher crystalline structure and grain growth led to a decrease in surface area.
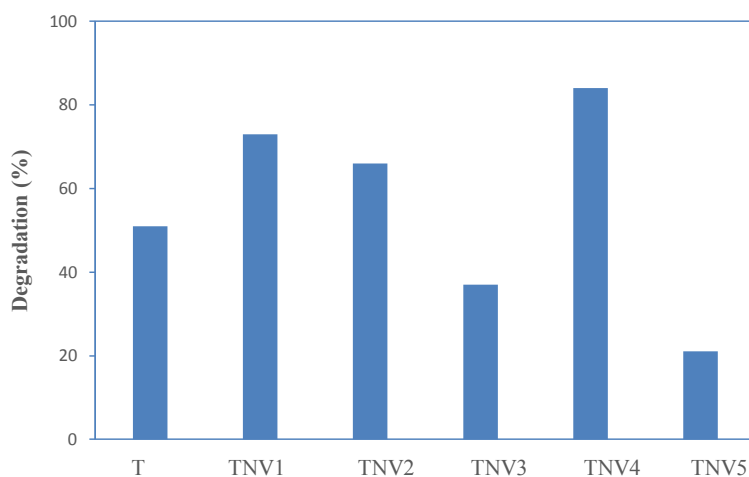


Fig. 2: Photocatalytic degradation of MB determined by pure and co-doped $TiO_2$ thin film after 1h UV irradiation.

Table 2: The physical properties of the Nb/V co-doped $TiO_2$ (TNV4) thin films calcined at different temperatures (calcination time = 1h).

| TNV4 | %A | %R | $d_A$ (nm) | $d_R$ (nm) | BET($m^2$/g) | η (%) |
|------|-----|-----|-----|-----|-----|-----|
| T= 475 °C | 100 | -- | 11.1 | -- | 158.2 | 84 |
| T= 575 °C | 73.4 | 26.6 | 18.2 | 32.3 | 132.6 | 93 |
| T= 675 °C | 41.5 | 58.5 | 22.3 | 52.4 | 56.8 | 67 |

The degradation efficiency for TNV4 nanocrystalline thin film at 575 °C is higher than that of TNV4-475 °C and TNV4-675 °C films (Table 2, $\eta_{575} > \eta_{475} > \eta_{675}$), showing a maximum for TNV4-575 °C. The maximum degradation is about 93% for TNV4-575 °C sample.

With increasing calcination temperature, the photocatalytic activity of thin films increases and reaches the maximum value at 575 °C. The increase in photocatalytic activity is due to the formation of anatase/rutile and the improvement of crystallization of two phases in the films.
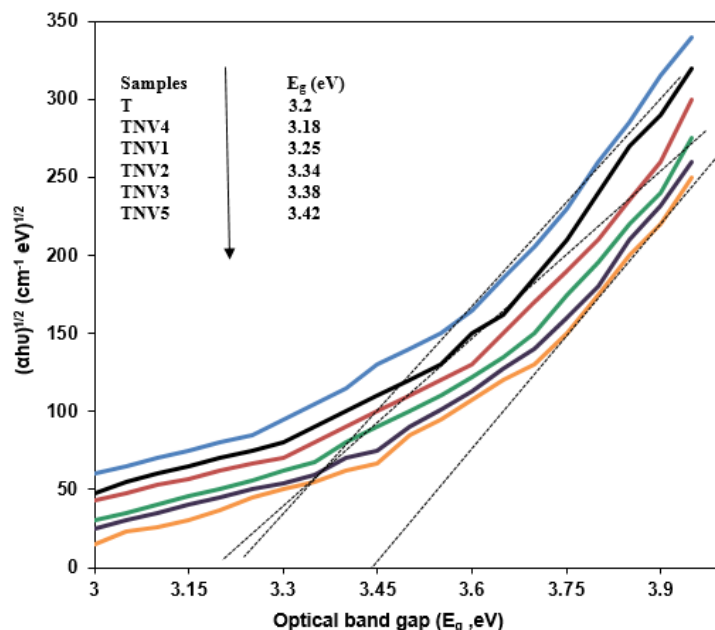


Fig. 3: $(\alpha h\nu)^{1/2}$ versus $h\nu$ plots for pure and co-doped $TiO_2$ thin film.
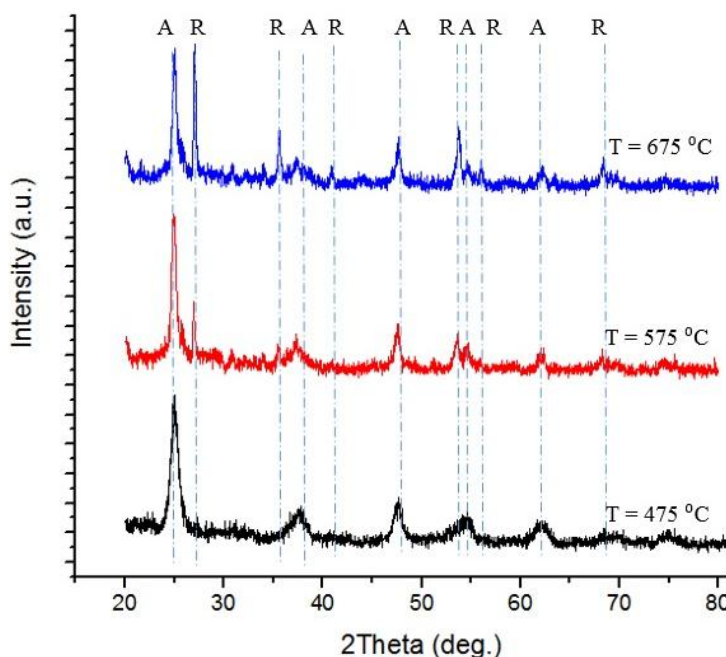


Fig. 4: XRD patterns of the TNV4 (5%Nb-15%V) thin film calcined at different temperatures (A: Anatase, R: Rutile).
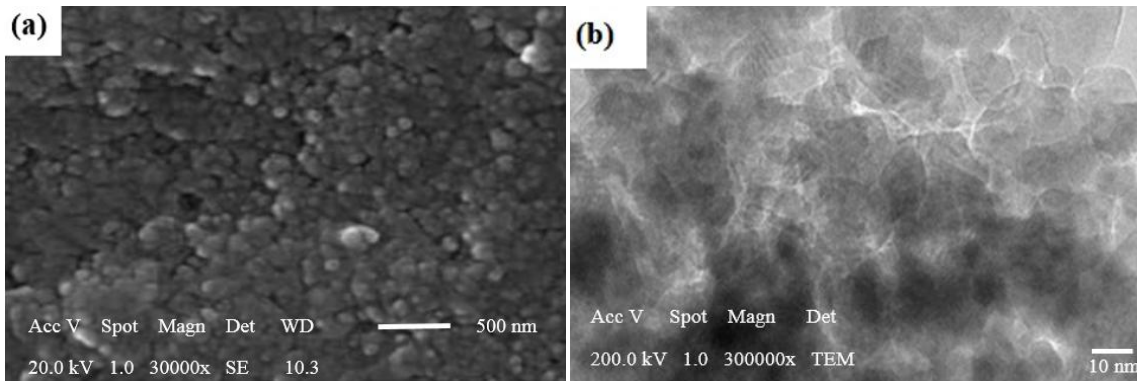
Fig. 5: SEM surface micrographs (a) and TEM image (b) of TNV4 thin film deposited on glass substrate that calcined at 475 ˚C for 1h.
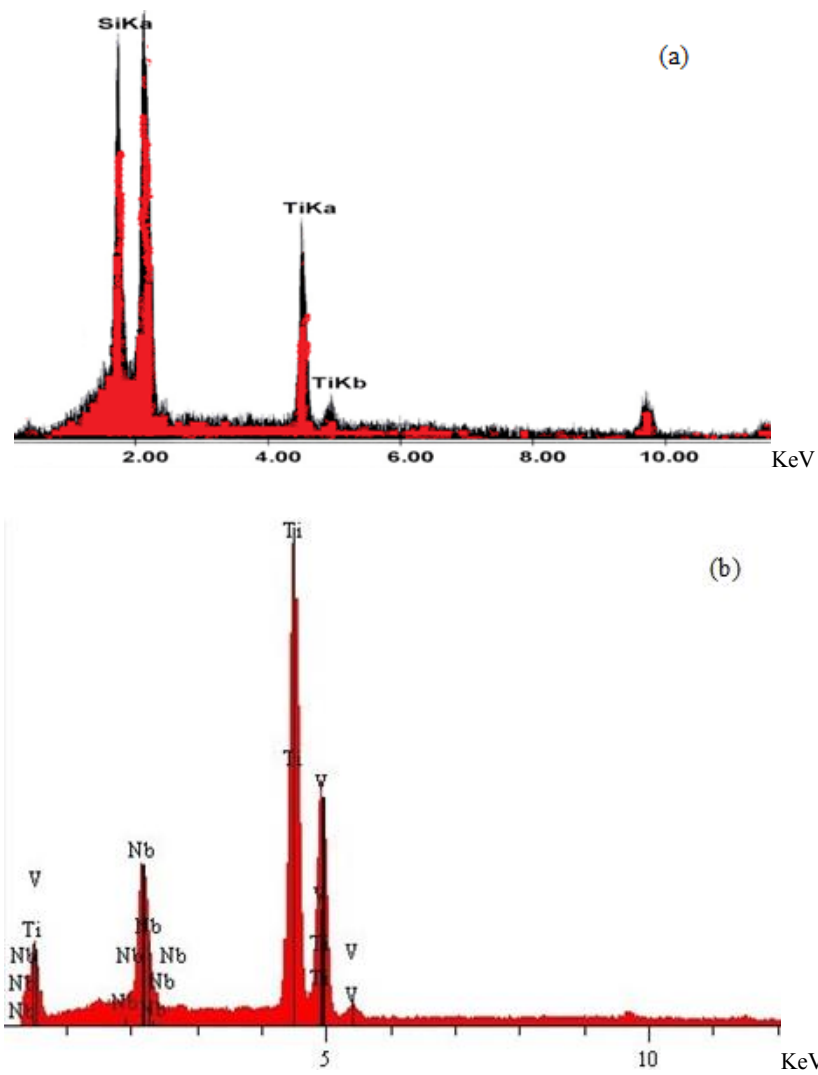


Fig. 6: EDX images of the pure TiO$_2$ thin film (T) (a) and TNV4 sample (b) calcined at 475 ˚C for 1h.

Therefore, due to their high specific surface areas and mix of two phases (Table 2, %A & %R), the photocatalytic activity of TNV4-575 °C thin films is higher than other thin films.

The enhancement in the photocatalytic activity is mainly caused by the changes in phase structures in films (as shown in Fig. 4), since calcination at 575 °C accelerates phase transformation from anatase to rutile and the crystallization of anatase. A composite of two phases of the same semiconductor and good crystallization of anatase lead to an improvement in photoactivity [42, 43].

The coupling of two phases allows the vectorial displacement of electrons from anatase to rutile phase and holds back the recombination of the electron–hole pairs in anatase [44]. Upon UV excitation, photo-generated electrons accumulate in the lower conduction band of rutile, whereas holes can accumulate in the valence bands of both anatase and rutile, since their valence bands are almost at the same level. Accumulated electrons in the conduction band of rutile can be transferred to oxygen adsorbed on the surface to form  or [44]. Accumulation of holes in the valence band of anatase and rutile leads to the production of surface hydroxyl radicals OH, which are responsible for the oxidation decomposition of MB. In heterogeneous anatase/rutile $TiO_2$ system, photo-generated electrons are effectively accumulated in the rutile phase, without recombining with holes in the anatase valence band, which leads to the enhancement in photocatalytic activity of anatase. The better crystallinity of anatase in $TiO_2$ calcined at 575 °C is also beneficial to the photocatalytic activity.

Fig. 5 shows SEM (Fig. 5a) and TEM (Fig. 5b) images of TNV4 thin film (T = 475 °C) with improved photo-catalytic activity. The film surfaces are smooth, homogeneous, and without cracks. Particle shape is generally spherical and similar to each other. Moreover, the surface consists of small granular crystallites with a size range of 10-15 nm (Fig. 5b) that is similar with that measured from XRD results. Synthesized films without agglomeration and big clusters causes an increase in specific surface area, and subsequently enhances desired photocatalytic properties of thin films.

Energy dispersive X-ray spectrometry (EDX) analysis of $TiO_2$ thin films at 475 °C shows characteristic peaks for Ti element (Fig. 6a). There is no trace of any other impurities within the detection limit of the EDX as shown in Fig. 6a.

The niobium and vanadium ions are incorporated into the structure of $TiO_2$ thin film (Fig. 6b) which has been confirmed by EDX analysis. No impurities were observed in the samples.

## CONCLUSIONS

The Nb/V co-doped $TiO_2$ thin film was prepared through sol−gel dip coating method and evaluated in terms of performance by the degradation rate of the MB aqueous solution under UV irradiation. The co-doped prepared samples showed an increase in the photoactivity.

The size of the crystallites in doped $TiO_2$ samples is smaller than those in undoped samples. This result suggests that dopants have an inhibiting role on the grain growth. Grain growth decreases mainly causes by dopant segregation at high solution energy zones like grain boundaries and outer surfaces of titania crystallites and particles, which indicates dopant distribution through vapor phase transport and grain boundary diffusion. The XRD pattern showed the anatase phase in $TiO_2$ calcined at 475°C with reduction of particle size by increasing dopant concentration in the samples; with the increase in surface area measured via BET, caused by the decrease in the particle size and increase in the surface area. Samples showed an increase in the surface hydroxyl groups, and reduction of recombination of e− and h+ assisted the enhanced activity of the catalyst toward degradation of MB by the synergistic effect of both Nb/V doping in $TiO_2$ thin film. The maximum photocatalytic efficiency under UV irradiation was measured for the TNV4 (5%Nb, 15%V) calcined at 475 °C.

## CONFLICT OF INTEREST

The authors declare that there is no conflict of interests regarding the publication of this manuscript.

## REFERENCES

[1] Fujishima A., Honda K., (1972), Electrochemical photolysis of water at a semiconductor electrode. *Nature.* 238: 37-38.
[2] Samuneva B., Kozhukharov V., (1993), Sol-gel processing of titanium-containing thin coatings. *J. Mater. Sci.* 28: 2353-2360.
[3] Wang C. Y., Liu C. Y., Shen T., (1997), The photocatalytic oxidation of phenylmercaptotetrazole in $TiO_2$ dispersions. *J. Photochem. Photobiol. A. Chem.* 109: 65-70.
[4] Palmer F. L., Eggins B. R., Coleman H. M., (2002), The effect of operational parameters on the photocatalytic degradation of humic acid. *J. Photochem. Photobiol.* 148: 137-143.
[5] Hoffmann M. R., Martin S. T., Choi W., Bahnemann D. W., (1995), Environmental applications of semiconductor photocatalysis. *Chem. Rev.* 95: 69-96.

[6] Ohko Y., Fujishima A., Hashimoto K., (1998), Kinetic analysis of the photocatalytic degradation of gas-phase 2-propanol under mass transport-limited conditions with a $TiO_2$ film photocatalyst. *J. Phys. Chem. B*. 102: 1724-1729.

[7] Herrmann J. M., (1999), Heterogeneous photocatalysis: Fundamentals and applications to the removal of various types of aqueous pollutants. *Catal. Today.* 53: 115-129.

[8] Lin J., Yu J. C., Lo D., Lam S. K., (1999), Photocatalytic activity of rutile $Ti_{1-x}Sn_xO_2$ solid solutions. *J. Catal.* 183: 368-372.

[9] Maruska H. P., Ghosh A. K., (1978), Photocatalytic decomposition of water at semiconductor electrodes. *Sol. Energy.* 20: 443-458.

[10] Bickley R., Gonzalez-Carreno T., Lees J., Palmisano L., Tille R. J., (1991), A structural investigation of titanium dioxide photocatalysts. *J. Solid State Chem.* 92: 178-190.

[11] Yu J., Yu J., Ho W., Jiang Z., (2002), Effects of calcination temperature on the photocatalytic activity and photo-induced super-hydrophilicity of mesoporous $TiO_2$ thin films. *New J. Chem.* 26: 607-613.

[12] Peng Y. H., Huang G. F., Huang W. Q., (2010), Visible-light absorption and photocatalytic activity of Cr-doped $TiO_2$ nanocrystal films. *Adv. Powder Technol.* 23: 8-12.

[13] Barakat M. A., Schaeffer H., Hayes G., Ismat-Shaha S., (2004), Photocatalytic degradation of 2-chlorophenol by Co-doped $TiO_2$ nanoparticles. *App. Catal. B: Environ.* 57: 23–30.

[14] Silva A. M. T., Silva C. G., Drazic G., Faria J. L., (2009), Ce-doped $TiO_2$ for photocatalytic degradation of chlorophenol. *Catal. Today.* 144: 13-18.

[15] Rauf M. A., Meetani M. A., Hisaindee S., (2011), An overview on the photocatalytic degradation of azo dyes in the presence of $TiO_2$ doped with selective transition metals. *Desalination.* 276: 13–27.

[16] Kocí K., Mateju K., Obalová L., Krejcíková S., Lacny Z. ´, Plachá D., Capek L., Hospodková A., Solcov O., (2010), Effect of silver doping on the $TiO_2$ for photocatalytic reduction of $CO_2$. *Appl. Catal. B: Environ.* 96: 239-244.

[17] Li Y., Xie C., Peng S., Lu G., Li S., (2008), Eosin Y-sensitized nitrogen-doped $TiO_2$ for efficient visible light photocatalytic hydrogen evolution. *J. Mol. Catal. A: Chem.* 282: 117–123.

[18] Janitabar Darzi S., Mahjoub A. R., Bayat A., (2016), Synthesis and characterization of visible light active S-doped $TiO_2$ nanophotocatalyst. *Int. J. Nano Dimens.* 7: 33-40.

[19] Rastkar Ebrahimzadeh A., Abbasi M., Jahanbin Sardroodi J., Afshari S., (2015), Density functional theory study of the adsorption of $NO_2$ molecule on Nitrogen-doped $TiO_2$ anatase nanoparticles. *Int. J. Nano Dimens.* 6: 11-17.

[20] Zakeri S. M. E., Asghari M., Feilizadeh M. Vosoughi M., (2014), A visible light driven doped $TiO_2$ nanophotocatalyst: Preparation and characterization. *Int. J. Nano Dimens.* 5: 329-335.

[21] Abbasi A., Jahanbin Sardroodi J., (2016), A theoretical study on the adsorption behaviors of ammonia molecule on N-doped $TiO_2$ anatase nanoparticles: Applications to gas sensor devices. *Int. J. Nano Dimens.* 7: 349-359.

[22] Hirano M., Nakahara N., Ota K., Tanaike O., Inagaki N., (2003), Photoactivity and phase stability of $ZrO_2$-doped anatase-type $TiO_2$ directly formed as nanometer-sized particles by hydrolysis under hydrothermal conditions. *J. Solid State Chem.* 170: 39-47.

[23] Kim J., Song K. C., Foncillas S., Pratsinis S., (2001), Dopants for synthesis of stable bimodally porous titania. *J. Eur. Ceram. Soc.* 21: 2863-2872.

[24] Akhtar M. K., Pratsinis S. E., Mastrangelo S. V. R., (1992), Dopants in vapor-phase synthesis of titania powders. *J. Am. Ceram. Soc.* 75: 3408–3416.

[25] Karakitsou K. E., Verykios X. E., (1993), Effects of altervalent cation doping of titania on its performance as a photocatalyst for water cleavage. *J. Phys. Chem.* 97: 1184-1189.

[26] Mu W., Herrmann J. M., Pichat P., (1989), Room temperature photocatalytic oxidation of liquid cyclohexane into cyclohexanone over neat and modified $TiO_2$. *Catal. Lett.* 3: 73-84.

[27] Choi W., Termin A., Hoffmann M. R., (1994), The role of metal Ion dopants in quantum-sized $TiO_2$: Correlation between photoreactivity and charge carrier recombination dynamics. *Phys. Chem.* 98: 13669-13679.

[28] Okada K., Yamamoto N., Kameshima Y., Yasumori A., MacKenzie K., (2001), Effect of $SiO_2$ addition on the anatase-to-rutile phase transition. *J. Am. Ceram. Soc.* 84: 1591-1596.

[29] Bsiri N., Zrir M. A., Bardaoui A., Bouaïcha M., (2016), Morphological, structural and ellipsometric investigations of Cr doped $TiO_2$ thin films prepared by sol–gel and spin coating. Ceram. Int. 42: 10599-10607.

[30] Iida Y., Ozaki S., (1961), Grain growth and phase transformation of titanium oxide during calcinations. *J. Am. Ceram. Soc.* 44: 120-127.

[31] Chao H. E., Yun Y. U., Xingfang H. U., Larbot A., (2003), Effect of silver doping on the phase transformation and grain growth of sol-gel titania powder. *J. Europ. Ceram. Soc.* 23: 1457-1464.

[32] Baker R. W., (2004), Membrane technology and application: Wiley Pub, Chichester.

[33] Klug P., Alexander L. E., (1974), X-Ray Diffraction Procedures, Wiley, New York.

[34] Sharma R., Bhatnagar M. C., (1999), Improvement of the oxygen gas sensitivity in doped $TiO_2$ thick films. *Sens. Actuators B*. 56: 215-219.

[35] Lai C. W., Sreekantan S., (2013), Study of $WO_3$ incorporated $C-TiO_2$ nanotubes for efficient visible light driven water splitting performance. *J. Alloys Compd.* 547: 43–50.

[36] Zhang Z., Shao C., Zhang L., Li X., Liu Y., (2010), Electrospun nanofibers of V-doped $TiO_2$ with high photocatalytic activity. *J. Colloid Interface Sci.* 351: 57–62.

[37] Garadkar K. M., Patil A. A., Hankare P. P., Chate P. A., Sathe D. J., Delekar S. D., (2009), $MoS_2$: Preparation and their characterization. *J. Alloys and Comp.* 487: 786-789.

[38] Yang Y., Chen X., Feng Y., Yang G.W., (2007), Physical mechanism of blue-shift of UV luminescence of a single pencil-like ZnO nanowire. *Nano. Lett.* 7: 3879–3883.

[39] Hu L., Yoko T., Kozuka H., Sakka S., (1992), Effects of solvent on properties of sol—gel-derived $TiO_2$ coating films. *Thin. Solid. Films.* 219: 18–23.

[40] Wang Z., Helmersson U., Käll P. O., (2002), Optical properties of anatase $TiO_2$ thin films prepared by aqueous sol–gel process at low temperature. *Thin Solid Films.* 405: 50-54.

[41] Yu J. G., Zhou M. H., Cheng B., Zhao X. J., (2006), Preparation, characterization and photocatalytic of in situ N, S-co-doped $TiO_2$ powders. *J. Mol. Catal. A*. 246: 176-184.

[42] Yu J. C., Yu J. G., Ho W. K., Zhang L. Z., (2001), Preparation of highly photocatalytic active nano-sized $TiO_2$ particles via ultrasonic irradiation. *Chem. Commun.* 19: 1942-1943.

[43] Yu J. C., Yu J. G., Ho W. K., Zhang L. Z., (2002), Photocatalytic activity of nano-sized $TiO_2$ powders by sol-gel method, using titanium tetraisopropoxide and EtOH/ $H_2O$ Solution. *J. Photochem. Photobiol. A*. 148: 263-271.

[44] Miyauchi M., Nakajima A., Hashimoto K., Watanabe T., (2000), A highly hydrophilic thin film under 1 μW/cm² UV Illumination. *Adv. Mater*. 12: 1923-1927.